BIOCHEMISTRY
including biophysical chemistry & molecular biology

Article

pubs.acs.org/biochemistry

Molecular Mechanism of Na^+,K^+-ATPase Malfunction in Mutations Characteristic of Adrenal Hypertension

Wojciech Kopec,[†] Bastien Loubet,[†] Hanne Poulsen,[‡,§,∥] and Himanshu Khandelia*[,†]

[†]MEMPHYS—Center for Biomembrane Physics, University of Southern Denmark, Campusvej 55, DK-5230 Odense M, Denmark

[‡]PUMPkin—Centre for Membrane Pumps in Cells and Disease, Danish National Research Foundation, Aarhus University, DK-8000 Aarhus C, Denmark

[§]Department of Molecular Biology, Aarhus University, Gustav Wieds Vej 10C, DK-8000 Aarhus C, Denmark

[∥]DANDRITE—Danish Research Institute for Translational Neuroscience, Nordic-EMBL Partnership of Molecular Medicine, Aarhus University, DK-8000 Aarhus C, Denmark

S *Supporting Information*

ABSTRACT: Mutations within ion-transporting proteins may severely affect their ability to traffic ions properly and thus perturb the delicate balance of ion gradients. Somatic gain-of-function mutations of the Na^+,K^+-ATPase α1-subunit have been found in aldosterone-producing adenomas that are among the causes of hypertension. We used molecular dynamics simulations to investigate the structural consequences of these mutations, namely, Leu97 substitution by Arg (L97R), Val325 substitution by Gly (V325G), deletion of residues 93−97 (Del93−97), and deletion−substitution of residues 953−956 by Ser (EETA956S), which shows inward leak currents under physiological conditions. The first three mutations affect the structural context of the key ion-binding residue Glu327 at binding site II, which leads to the loss of the ability to bind ions correctly and to occlude the pump. The mutated residue in L97R is more hydrated, which ultimately leads to the observed proton leak. V325G mimics the structural behavior of L97R; however, it does not promote the hydration of surrounding residues. In Del93−97, a broader opening is observed because of the rearrangement of the kinked transmembrane helix 1, M1, which may explain the sodium leak measured with the mutant. The last mutant, EETA956S, opens an additional water pathway near the C-terminus, affecting the III sodium-specific binding site. The results are in excellent agreement with recent electrophysiology measurements and suggest how three mutations prevent the occlusion of the Na^+,K^+-ATPase, with the possibility of transforming the pump into a passive ion channel, whereas the fourth mutation provides insight into the sodium binding in the E1 state.

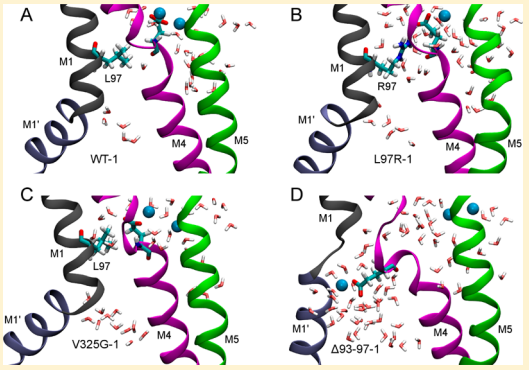

The Na^+,K^+-ATPase (NKA) is an essential transmembrane protein of the P-type pump family and serves as a primary active ion transporter in all eukaryotic cells.[1−3] Fueled by ATP, NKA exchanges three intracellular Na^+ ions with two extracellular K^+ ions for one hydrolyzed ATP molecule, thereby maintaining proper ion gradients across plasma membranes.[4,5]

According to the classical Post−Albers reaction cycle,[6,7] NKA activity is described in terms of the alternating-access model, and the pump conformation switches between inside-open E1 and outside-open E2 states together with phosphorylated intermediates E1P and E2P. Until very recently, the only resolved X-ray crystal structures of NKA were those of the potassium-bound occluded E2 state,[8−10] which precisely identified ion-binding sites I and II. Recently, the crystal structure of an ouabain-bound, ion-free equivalent of the E2P outside open state was solved.[11] The availability of this structure has allowed for studies of, for example, external ion-binding pathways.

Mutations within the NKA α2 and 3 subunits cause the diseases rapid-onset dystonia parkinsonism, alternating hemiplegia of childhood, and familial hemiplegic migraine type 2.[12] Recently, novel gain-of-function mutations were found in the NKA α1 subunit of adrenal aldosterone-producing adenomas (APAs) that occur in at least 5% of patients with hypertension.[13,14] The mutations were L97R substitution, V325G substitution, 93−97 deletion, and EETA956S deletion−substitution.[13] L97R, V325G, and Del93−97 are close to the important Glu327 ion-binding residue of ion-binding site II,[8] whereas EETA956S may influence sodium-specific binding site III.[15] Strikingly, L97R and the 93−97 deletion were found in the majority of patients, making L97 a clear hotspot for APA-specific pump mutations.

In this article, we report atomic-level molecular dynamics (MD) simulations to grasp the structural mechanism of pump dysfunction. The impact of the mutants on the ion-binding

Received: October 18, 2013
Revised: January 8, 2014
Published: January 15, 2014

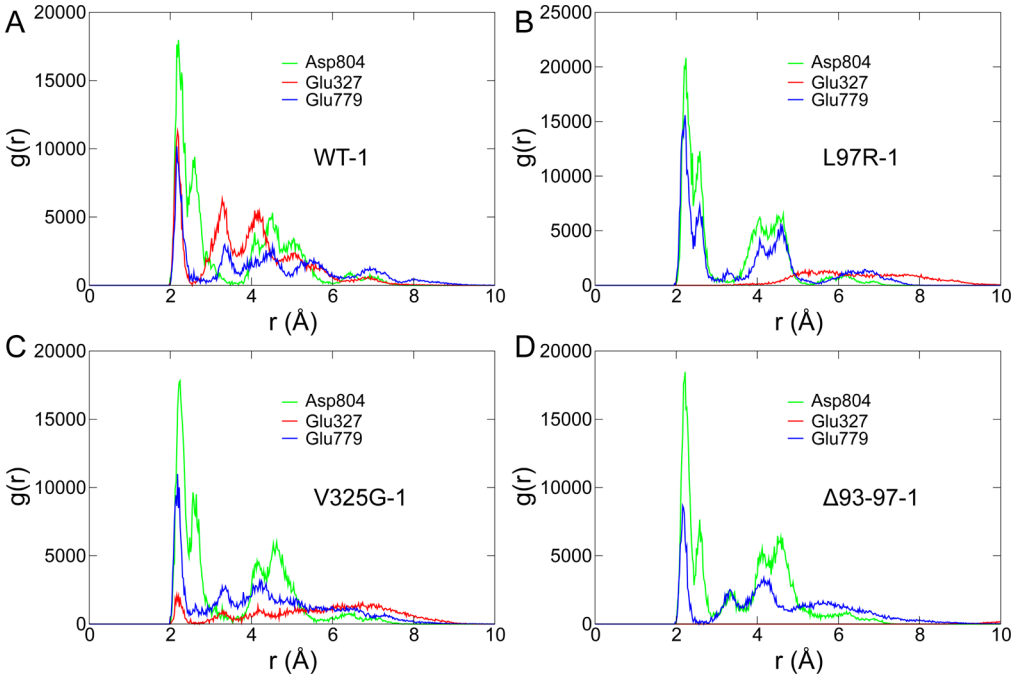

Figure 1. Radial distribution functions between the bound sodium ion in site I and protein residues important for ion binding. Results for (A) the WT-1 system, (B) L97R-1, (C) V325G-1, and (D) Δ93−97-1. Glu327 participates in binding only in the WT.

process is likely to be captured by simulations with the novel structure of an E2P, ouabain-bound state of NKA because all mutants are sensitive to ouabain,[13] meaning that mutants are able to attain either this state or the close equivalent.

In previous work, we successfully used MD of various NKA mutants in the potassium-occluded E2 state to recognize a previously unknown ion pathway[16] and to describe the effect of pump phosphorylation caused by the protein kinase A.[17] Here, we report how the L97R, V325G, Del93−97, and EETA956S mutations affect the ion-binding process as well as water accessibility within the NKA transmembrane region and provide an appealing structural explanation of the inward current leak recorded in electrophysiology measurements. Leu97 is a residue of particular importance and is known to guide Glu327 toward binding site II, thereby controlling the extracellular gate of the ion-binding cavity.[18] Similarly, the Glu327 position may be controlled by mutation in its close proximity, which changes the geometry of the helix. We show how the interaction network of Glu327 is distorted by the disease-causing mutations L97R, V325G, and Del93−97 and how this affects protein function. Finally, we also present how the EETA956S mutation affects the putative III sodium binding site as a result of the deletion of the key Glu954 residue and its surrounding residues. Our results are in excellent agreement with experiments and help to understand the molecular background of adrenal hypertension, which ultimately might pave the way toward novel drugs or diagnostic methods for this disease.

METHODS

All-atom MD simulations were implemented with the recently solved pig kidney $\alpha\beta$ dimer of NKA (PDB code 4HYT)[11] embedded in a fully hydrated 110 × 110 × 192 Å^3 1-palmitoyl-2-oleoyl-*sn*-glycero-3-phosphocholine (POPC) lipid bilayer. POPC is a routinely used lipid in simulations of transmembrane proteins, such as ion pumps[19,20] and ion channels,[21] and has proven to be successful in modeling the properties of biological membranes and their impact on embedded proteins.[22]

Simulations were performed using GROMACS version 4.6.1,[23−26] employing CHARMM27 force-field parameters for proteins and sodium ions[27−29] and the CHARMM36 force field for phospholipids.[30,31] Water was modeled using the TIP3P model.[32] Periodic boundary conditions were applied in all three directions. A neighbor list with a 13 Å cutoff was used for nonbonded interactions and is updated every 10 steps. The van der Waals interactions were switched off from 8 to 12 Å. The particle mesh Ewald (PME)[33,34] method with a 13 Å cutoff was employed for the treatment of electrostatic interactions. The simulated systems were maintained at 298 K and 1 bar according to the NPT statistical ensemble. Temperature coupling was performed using a Berendsen thermostat[35] for equilibration runs and a Nose−Hoover thermostat[36,37] for production runs, which was carried out separately for the solute (protein and lipids) and the solvent (ions and water molecules). A semiisotropic pressure coupling was applied using the Berendsen barostat[35] for equilibration runs and the Parrinello−Rahman barostat[38,39] for production runs. The SHAKE algorithm was employed to constrain all hydrogen-containing covalent bonds, which allows a time step of 2 fs. Trajectories were sampled every 10 ps.

The starting structure for WT NKA was obtained from the crystal structure by deleting the bound ouabain steroid and the Mg^{2+} ion bound to the ion-binding sites. After a short equilibration, the enzyme structure represents an approximation of the E2P phosphorylated state of the pump (i.e., open to the extracellular side and with no ions bound). Water molecules and ions spontaneously enter the binding sites during simulations. All residue numbering follows the sequence of the pig kidney protein. Asp926 and Glu954 were kept protonated, as argued previously.[16] Asp369 was phosphorylated, with parameters taken from Damjanović et al.[40] The starting structures of the L97R and V325G mutants were

dx.doi.org/10.1021/bi401425g | *Biochemistry* 2014, 53, 746−754

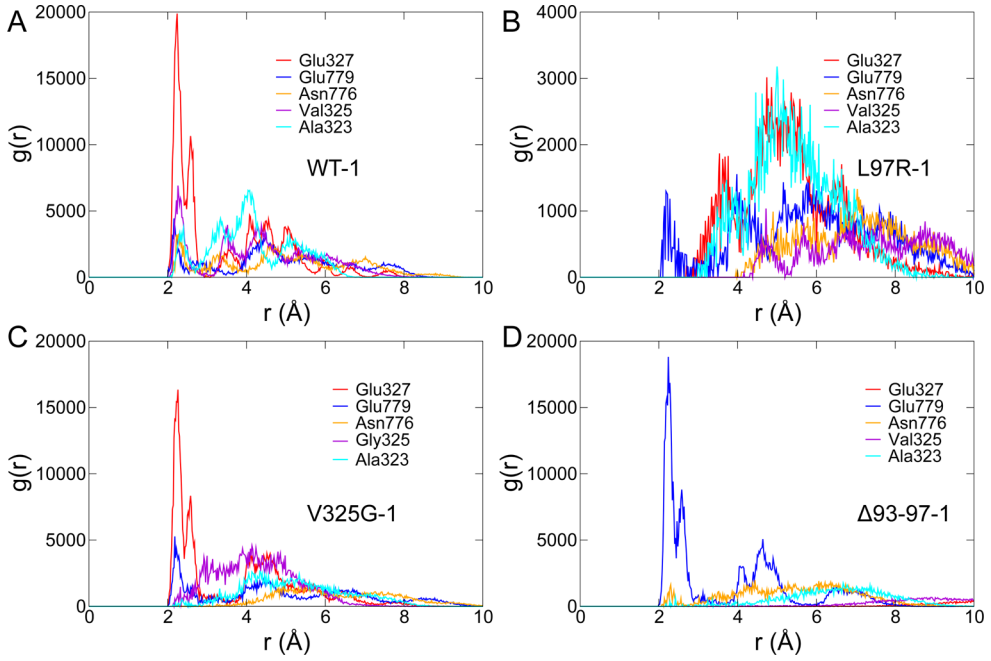

Figure 2. Radial distribution functions between the bound sodium ion in site II and protein residues important for ion binding. Results for (A) the WT-1 system, (B) L97R-1, (C) V325G-1, and (D) Δ93−97-1.

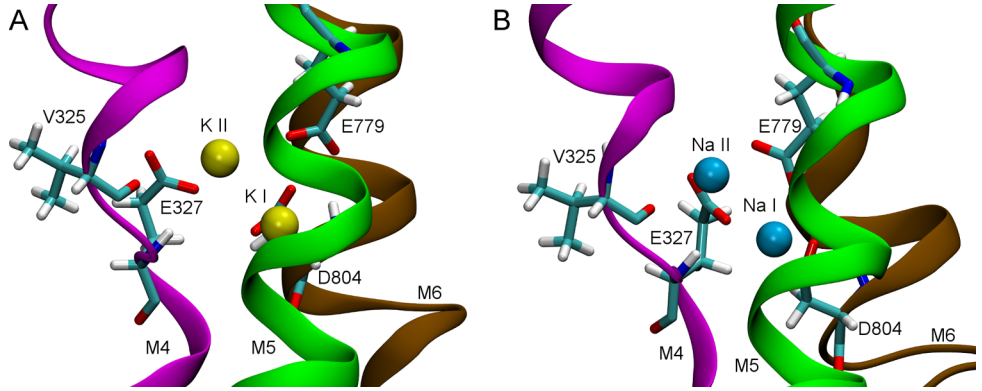

Figure 3. Sodium ions spontaneously bind to the correct binding sites in the WT simulations. Final simulation snapshot (t = 100 ns) showing the sodium ion in its binding site (B) compared to the position of potassium ions in crystal structure of the E2 state of Na^+,K^+-ATPase (PDB code 3A3Y, A). Potassium ions are shown as yellow spheres and sodium ions, as cyan spheres. A few important ion-binding residues are shown as licorice.

constructed using the mutagenesis wizard implemented in PyMol. The starting structure of Del93−97 was obtained by deleting residues 93−97 of the α-subunit in the WT protein. The starting structure of the EETA956S mutant was constructed by first substituting Ala956 residue by Ser956 and then by deleting the Glu953, Glu954, and Thr955 residues. The protonation states are the same in WT and L97R as well as in the V325G and Del93−97 mutants; however, in the EETA956S mutant, the protonated Glu954 residue is not present. Proteins were embedded in the POPC membrane using the g_membed procedure implemented in GROMACS.[41] The systems were hydrated with approximately 56 000 water molecules and kept electrostatically neutral by sodium ions randomly placed in the aqueous phase. We used only sodium in the medium despite the fact that NKA in the E2P state releases sodium and binds potassium. In simulations of the WT with potassium, the observations were identical with respect to the spontaneous ion binding and binding sites (data not shown, manuscript in preparation).

After 5000 steps of energy minimization with steepest descent method and a subsequent 10 ns equilibration, two copies of 100 ns MD simulations were performed for WT (WT-1, WT-2), L97R (L97R-1, L97R-2), V325G (V325G-1, V325G-2), Del93−97 (Δ93−97-1, Δ93−97-2), and EETA956S (EETA956S-1, EETA956S-2). The analysis was carried out using GROMACS programs, the HOLE package,[42] and home-made scripts. Visualizations and snapshots were rendered using VMD[43] and the MOLE online server[44] for pore visualizations.

RESULTS

We simulated the novel E2P state stripped of Mg^{2+} and ouabain in a POPC membrane and with sodium ions in the water (corresponding to a 10 mM sodium concentration). The root-mean-square deviations (rmsd) of Cα atoms relative to the crystal structure slightly exceed 5 Å in all simulations (data not shown) because of large movements of the A and N domains and of the β-subunit. Importantly, the rmsd for the trans-membrane region of the protein does not exceed 2 Å for most

dx.doi.org/10.1021/bi401425g | Biochemistry 2014, 53, 746−754

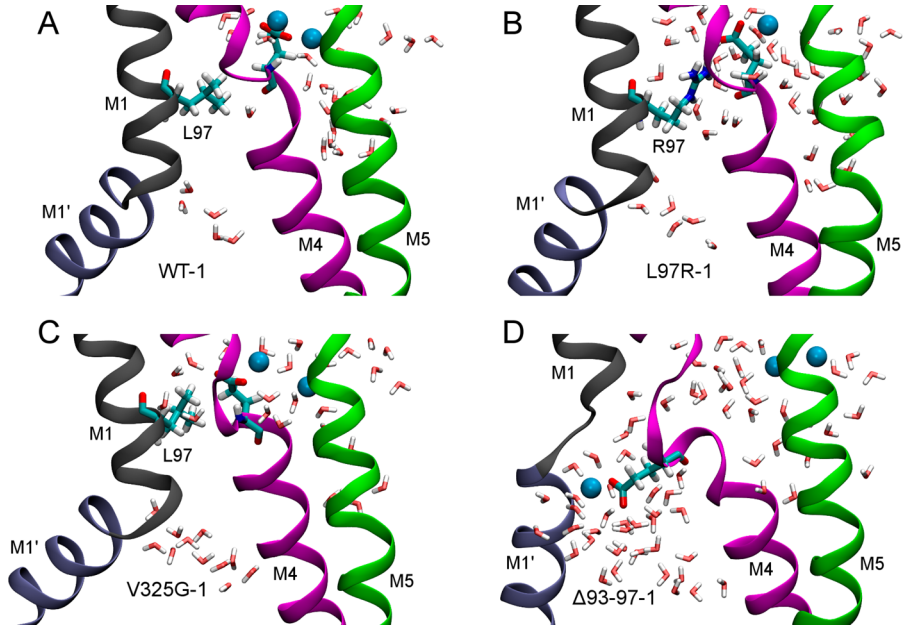

Figure 4. Representative simulation snapshots showing overall changes near and in the ion-binding domain. Glu327 interacts with Arg97, and the pair becomes hydrated in L97R-1 (B); similarly, Glu327 is placed near Leu97 in V325G-1 by the M4 helix distortion (C); the intracellular pathway opens in Δ93−97-1 (D) because of the shortening of the M1 helix (black cartoon) and the M1′ helix rearrangement (ice-blue cartoon). Sodium ions are shown as cyan spheres. Water molecules within 12 Å of Glu327 (A−C) or Pro326 (D) are shown as red and white licorice. Glu327 and Leu97 (A, C) or Arg97 (B) are shown as licorice. An additional sodium ion is attracted by Glu327 in Δ93−97-1 from the intracellular side.

of the simulation time even though this domain spontaneously binds sodium ions in simulations, as described later. Each of the systems (WT, L97R, V325G, Δ93−97, and EETA956S) was simulated twice, and the two copies are identical in most respects. Therefore, the figures herein only show data from one of the simulations. The corresponding graphs for the other copy are available in the Supporting Information.

Spontaneous Na^+ Binding in WT. During both WT simulations, two sodium ions spontaneously enter ion-binding sites I and II from the extracellular side within 20 ns and remain stable within the binding pockets over the entire simulation time. Binding site I, located deeper in the protein, is occupied first followed by subsequent binding to site II.

Radial distribution functions (RDFs) (Figures 1 and 2 and Supporting Information Figures 1 and 2) show that the ions are tightly coordinated in binding site I by M5 Glu779, M6 Asp804, and M4 Glu327 and in binding site II by M4 Glu327, Val325, Ala323, M5 Glu779, and M5 Asn776. The ions are positioned similar to the potassium ions in the crystal structure of the E2 occluded state of NKA (PDB code 3A3Y), as shown in Figure 3. Minor differences arise because sodium is significantly smaller than potassium (sodium's effective ionic radius is 1.02 Å, whereas potassium's effective ionic radius is 1.38 Å),[45] from dynamic fluctuations that are averaged out in the crystal structure, and because we are not simulating the potassium-occluded state.

Changes in Na^+ Binding upon Mutations. Structurally, the L97R, V325G and Del93−97 mutations are very close to an essential binding residue in M4, Glu327,[8] and they directly influence the ion-binding process and ion coordination.[18] The EETA956S mutant is located on the other side of the α-subunit, near sodium-specific ion-binding sites IIIa and IIIb that do not bind an ion in the E2P state of the protein; therefore, this mutation does not affect ion binding in the simulated state (data not shown).

In the L97R simulations, the Glu327 side chain rotates toward M1 and interacts via a salt bridge with positively charged Arg97 (Figure 4). Movement of Glu327 compromises the optimal geometry of binding site II. In L97R-1, the first ion binds after 60 ns, but the second sodium ion binds only after 80 ns and periodically enters and leaves binding site II. In L97R-2, the first sodium binds after 40 ns, whereas the second still did not bind after a 100 ns simulation (Figures 1 and 2 and Supporting Information Figures 1 and 2). The binding at site I is analogous to that in the WT (without contribution from Glu327 for the mutant), although the presence of the positively charged Arg97 side chain near binding site II weakens the electrostatic attraction between the protein and ions. Interestingly, the M1 and M4 helices are positioned similarly in the L97R and WT simulations. (Figure 4).

In the relatively mild V325G mutation, both ions are able to bind quickly to their respective binding sites (10 ns for site I and 40 ns for site II in V325G-1; 20 ns for site I and 50 ns for site II in V325G-2). Glu327 participates in binding only in site II (Figures 1 and 2 and Supporting Information Figures 1 and 2). Visual inspection (Figure 4) reveals that Glu327 is indeed moved away from site I because of the M4 helix distortion caused by the introduction of the poor-helix forming Gly residue. It is also reflected in Figure 5, which shows that Glu327 is located closer to Leu97 than it is in the WT and is somewhat similar to the L97R mutant.

The more drastic Del93−97 mutation alters the local environment within the protein significantly. The shortening of M1 by five residues forces its kinked part (M1′) and the loop connecting the two parts to rearrange at the water−membrane interface (Figure 4), and the resultant free volume is, to some degree, occupied by Glu327, which moves there by a shift in the M4 helix (Figure 4). As a result, not only does Glu327 stick out toward the intracellular side but also the positions of other M4 residues important for binding are altered and the ion-

dx.doi.org/10.1021/bi401425g | *Biochemistry* 2014, 53, 746−754

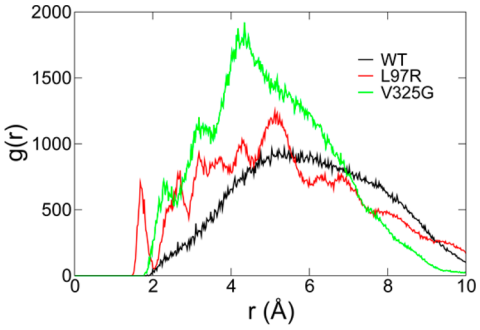

Figure 5. Radial distribution functions between residues Glu327 and Leu/Arg97. In L97R-1, Glu327 interacts strongly with Arg97 via a salt bridge, whereas in V325G-1, Glu327 is placed in the vicinity of Leu97 by the distortion of the M4 helix.

binding times are significantly longer in both simulations: the first ion binds after 60 ns and the second, after 80 ns. The ions have substantially more degrees of freedom and are coordinated mainly by the negatively charged residues Glu779 and Asp804 (Figures 1 and 2 and Supporting Information Figures 1 and 2).

The root-mean squared fluctuation values for the bound ions in WT-1, L97R-1, V325G-1, and Del93−97-1 are 0.12, 0.52, 0.24, and 0.40 Å, respectively, suggesting that the ions are tightly bound in the WT but not as much in the mutants. The observation that two ions can still bind in the Del93−97 systems may arise from the additional exposure of Glu779 and Asp804 to the extracellular ion pathway as a result of the movement of M4. Visual inspection (Figure 4) suggests that ions are able to penetrate deeper into the protein, toward putative sodium-binding site(s) III.[15]

Water Accessibility. In the WT, water molecules quickly enter the binding sites from the extracellular side, transporting ions (Figure 4). The hydration level of Leu/Arg97 was evaluated by calculating RDFs with water molecules (Supporting Information Figures 4 and 5). In WT and V325G simulations, Leu97 is kept dry because its hydrophobic side chain prevents water molecules from entering further into the protein.

In the L97R mutant, however, the situation is different. The hydrophilic Arg97 side chain attracts an additional water column from the extracellular side, which hydrates the interacting pair of Glu327 and Arg97, and water penetrates deeper into the protein along M1 (Figure 4), although the water column does not span both sides of the membrane.

The aforementioned movement of M1′ in Del93−97 systems creates a tunnel in the protein that is rapidly filled with water molecules from both sides of the membrane (Figures 4 and 6). The intracellular water path is formed between M1′ Glu91 and Gly92, M1 Trp98, and the side chain of Glu327. Glu327 remains hydrated, and water freely diffuses through the protein, across the membrane. Interestingly, in Del93−97-1, a sodium ion comes in from the intracellular side through the newly opened pathway and interacts with Glu327, showing that the intracellular pathway is permeable for sodium. The radius of the pore created by the deletion was measured by the HOLE package (Figure 6). In Del93−97 mutants, the radius of the pore in the most narrow part is ∼2 Å, allowing dehydrated sodium ions to flow in, whereas in the WT system, such a pore has a radius below 1 Å, indicating that the path is completely closed.

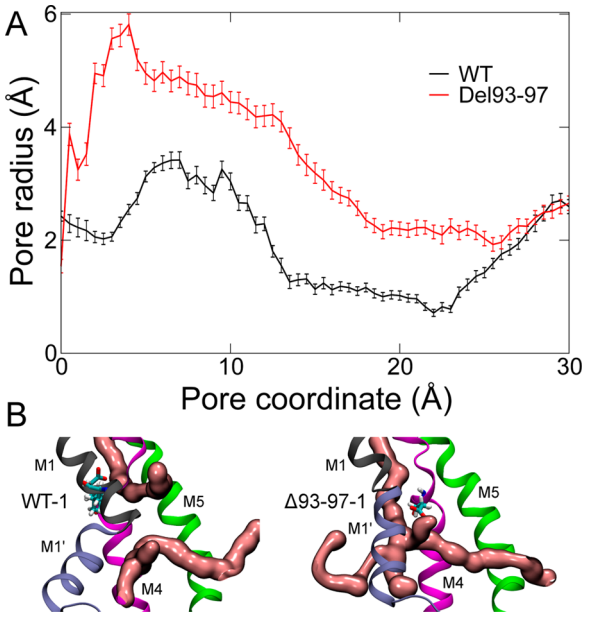

Figure 6. (A) Size of the pore between the M1 helix and the M4 helix that is defined along the line connecting residues Glu88 and Ile786. Zero-point of the pore coordinate is located on Glu88. The pore is small for the WT-1 system, whereas its size increases significantly in the Δ93−97−1 system, allowing ions and water molecules to flow. (B) Visualization of the pore superimposed with snapshots from Figure 4. Pores are shown as pink surfaces.

The ion-transporting extracellular water pathway in the WT reaches the protonated Glu954 residue (Figure 7), which is putatively involved in the III sodium-specific binding site in the E1 state of the pump. On the outer side of the protein, the side chain of the preceding residue, Glu953, is immersed in water because of the water defect on the intracellular membrane−protein interface. Upon EETA956S mutation, water from these two cavities joins together inside the protein, forming a continuous water pathway (Figure 7) that connects the extra- and intracellular sides of the membrane. The HOLE package detects a ∼2 Å widening of the entrance of the pore (Figure 8) in the EETA956S mutant compared to the WT. Interestingly, this new water pathway is in a close proximity to the C-terminus and ultimately may connect with the C-terminal ion pathway that is important for tuning the protonation states of Asp926 and Glu954, residues involved in the unique sodium binding site III.[16]

DISCUSSION

Here, we presented MD simulations that reveal the molecular background of the L97R, V325G, Del93−97, and EETA956S mutations within the NKA α1-subunit that occur in adrenal APAs in patients with hypertension. The simulations show that in the E2P state L97R, V325G, and Del93−97 mutations significantly alter the ion-binding process and ion coordination. Furthermore, L97R and Del93−97 promote hydration of regions near the mutated residues. The EETA956S mutant, located on the opposite side of the protein, does not influence ion binding in the E2P state. However, it opens a different water pathway throughout the pump, affecting sodium-specific binding site III.

The original protein structure file contains a bound ouabain molecule as well as an Mg^{2+} in binding site II. This magnesium ion stimulates ouabain binding, which in turn stabilizes the

dx.doi.org/10.1021/bi401425g | Biochemistry 2014, 53, 746−754

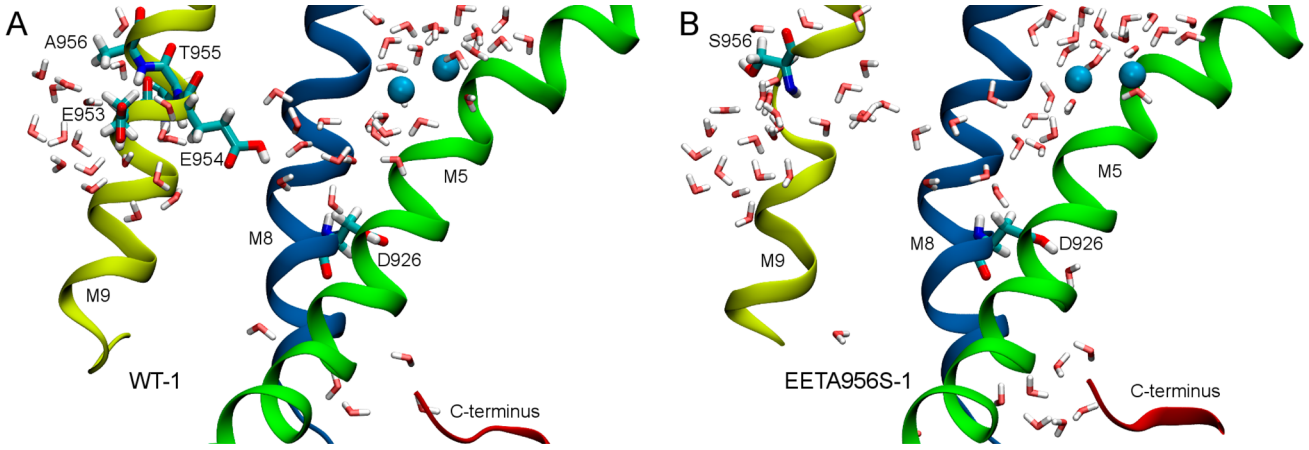

Figure 7. Representative simulation snapshots showing changes in the IIIa and IIIb ion-binding sites. Deletion of Glu953, Glu954, and Thr955 of the IIIa site opens an additional water pathway flowing through the protein. This water pathway lies in the proximity of the IIIb site and the C-terminus pathway. Mutated residues and Asp926 of the IIIb site are shown in licorice. The C-terminus is shown as a red ribbon. Bound sodium ions are shown as cyan spheres. Water molecules within 10 Å of Ala/Ser956 and Asp926 are shown as red and white licorice.

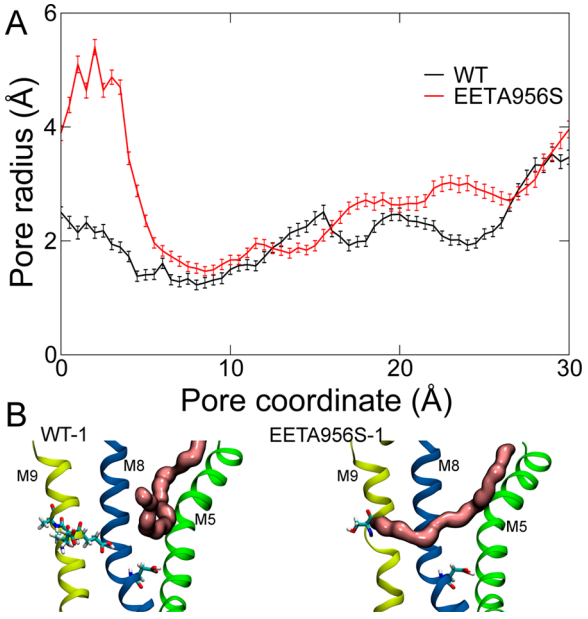

Figure 8. (A) Size of the pore on the M9 helix that is defined along the line connecting Gly950 and Glu779 residues. Zero-point of the pore coordinate is located on Gly950. The pore is small for the WT-1 system, whereas its size increases significantly in the EETA956S-1 system, allowing water molecules to flow. (B) Visualization of the pore superimposed with snapshots from Figure 7. Pores are shown as pink surfaces.

pump in the outside-open state.[11] Because NKA normally does not transport Mg^{2+}, we decided to remove it in our simulations together with the ouabain molecule. As a result, we obtained an ion-free model of the E2P state that is ready to bind extracellular ions. Of course, an artificial deletion of the positive charged ion will affect the binding site because of the electrostatic repulsion between negatively charged residues involved in binding. However, ion-binding sites I and II are quite flexible (e.g., they are able to bind bigger organic ions while remaining fairly undistorted);[46] therefore, we anticipate that the removal of the ion and subsequent equilibration would produce a structure similar to the physiologically relevant E2P state just after the dissociation of intracellular sodium. Ultimately, reported spontaneous ion binding at the correct binding sites in WT simulations reinforces the validity of using the oaubain-bound structure as a template to construct the first approximation of the E2P outside-open state model.

All ionizable residues involved in binding sites I and II were kept deprotonated, and sodium quickly bound the proper sites in the WT. Protonation of Glu327, Glu779, and Asp808 has been proposed to promote selectivity for potassium over sodium.[47] Simulations of NKA in the E2P state with different counterions and protonation states as well as the detailed characterization of ion-binding pathways will be discussed elsewhere (manuscript in preparation). Overall, sodium ions bind along a pathway similar to that proposed previously for the closely related calcium pump SERCA as the exit path for calcium ions.[48]

Our main goal was to investigate the molecular mechanism of the somatic gain-of-function mutations identified in hypertension-causing adenomas: the L97R and V325G substitutions, Del93−97 deletion, and EETA956S deletion−substitution. The mutants were previously characterized by electrophysiology for ion currents in intact *Xenopus* oocytes, showing an inward current leak in all mutations.[13] H^+ was the main current carrier in L97R and Na^+, in the Del93−97 mutant. Results for V325G mutants showed significantly smaller conductance, and we do not see any additional pathway opening in our simulations, indicating that the current leak is less likely. The partial hydration of the pathway in the L97R simulation and the intracellular sodium-accessible pathway in the Del93−97 simulation are in remarkable agreement with electrophysiology. On the basis of our results, it also seems likely that H^+ is the current carrier in EETA956S, as the pathway responsible for leaking includes the standard pathway for ion binding in the E2P state; therefore, metal ions bind correctly, leaving protons as the only possible carriers.

We also showed that monovalent ions are still able to bind L97R, V325G, and Del93−97 mutants because of the exposure of their anionic residues, although the ion coordination is significantly altered, particularly in binding site II. Mutation of the hydrophobic Leu97 residue, the so-called gatekeeper[49] of the extracellular gate, into positively charged arginine drags the negatively charged Glu327 side chain away from binding site II, preventing correct ion coordination and subsequently prevent-

dx.doi.org/10.1021/bi401425g | *Biochemistry* 2014, 53, 746−754

ing the occlusion of the pump. Very similar behavior of Glu327 is observed in the V325G mutant. The introduction of the small Gly residue compromises the optimal exposure of Glu327 by changing the geometry of the unwound part of M4 that is caused by conserved Pro326.[3] The interacting pair of charged residues, Arg97 and Glu327, in L97R gets rapidly surrounded by water molecules that penetrate deeper into the protein. Although we do not see a full water column spanning both sides of the membrane, such a water pathway can certainly open in a longer simulation, explaining the proton leak recorded in electrophysiology. Additionally, the polar Ser94 residue is located in proximity to Arg97, toward the intracellular side of the membrane. The serine side chain can be readily replaced by a water molecule or may facilitate proton transfer by the Gortthuss mechanism (proton hopping).

A distinct feature in almost all P-type ATPase crystal structures is the presence of a ∼90° kink of M1 (the angle between M1 and M1′ helices).[3] The kink has a putative role in ion selectivity because it is located at the entry of a cytoplasmic pathway.[49,50] A 12 Å sliding of M1 is thought to mediate the opening of the intracellular gate.[51,52] In the Del93−97 mutant, several important residues in the M1 helix are deleted, including the Leu97 gatekeeper as well as conserved Phe93 that might be important in the dehydration of sodium ions in the E1 state.[53] We observed the opening of the intracellular pathway because of the movement of M1′ relative to the shortened M1 helix (Figure 4). The newly opened pathway is permeable for both water and sodium ions. Taken together, we anticipate that the shortening of M1 and the rearrangement of M1′ to some extent mimics the sliding of M1 expected to occur during the E2−E1 transition. In Δ93−97-1, although a sodium ion approaches the pathway form the intracellular side, the ion flow would occur down the concentration and electrical gradients in vivo (i.e., from the extracellular to the intracellular side), which explains the electrophysiology measurements. In these mutants, Glu327 attracts sodium ions because it is located on the edge of the tunnel, closer to the M1 helix. The movement of Glu327 compromises the stability of binding site II, thus trapping the pump in the outside-open conformation and ultimately transforming it into a sodium channel that is still able to bind extracellular potassium but unable to transport it. However, electrophysiologically, Del93−97 mutants are not permeable for protons or potassium. The lack of potassium permeability may be explained in terms of the bigger ionic radius of a potassium ion, as ions are probably transported without their hydration shells (Figure 6). Nevertheless, the reason that protons are not accessible, because the pathway is permeable for water molecules and sodium ions, remains unknown.

EETA956S mutants respond to extracellular potassium with forward pumping in electrophysiology, which also agrees with our observation that this mutant does not influence ion binding from the extracellular side. When it comes to the binding from the intracellular side, the NKA is thought to have two different sites involved in binding the unique third sodium in the E1 state: IIIa and IIIb.[3] The EETA956S mutation directly compromises the IIIa site because of the deletion of the crucial Glu954 residue but also may influence the IIIb site (Figure 7). Because both of these sites work together with the C-terminus for the correct binding of the third sodium ion in the E1 state,[3] it is likely that the EETA956S mutation hampers such a binding. Despite this, experimental data suggest that the mutants are still functional, meaning that pumps are able to bind intracellular sodium and to occlude. This suggests that the E1P−E2P transition is possible even without completely correct binding of sodium to binding site III.

We note here that the length of our simulations (100 ns each) is short with respect to the time scale of the protein pumping cycle and related large conformational transitions, which take at least microseconds to milliseconds. Therefore, we remain extremely cautious in predicting long-scale structural changes based solely on simulation data. Instead, we focus on local rearrangements caused by mutations, which should have functional effects on the shorter time scale, whereas the longer-scale consequences might be anticipated in conjunction with experiments. The same reasoning applies to the observed spontaneous ion binding. However, the fact that we observe spontaneous ion binding in multiple simulations suggests that the simulation time is long enough for a qualitative description of the ion-binding changes in the NKA.

To conclude, we report for the first time spontaneous ion binding in the E2P state of the NKA ion pump as well as both structural and molecular mechanisms of gain-of-function NKA α1-subunit mutants identified in hypertension-causing adenomas. In agreement with very recent electrophysiology findings, we show how L97R, V325G, Del93−97, and EETA956S mutations affect NKA binding sites and lead to the opening of new water pathways. Moreover, we show how the rearrangements of the kinked M1′ helix open the intercellular ion pathway, which may be of particular importance in revealing the role of M1 and M1′ in sodium binding to the E1 state of the pump. Finally, we anticipate the effect of deleting one of the putative sodium binding sites III on the E1P−E2P transition. Further simulations studies await the availability of the crystal structure of the E1 or E1P states.

■ ASSOCIATED CONTENT

Supporting Information

Ion binding RDFs for the second, independent copy of the system; RDFs between Glu327 and Leu/Arg97 residues for the second copy; and hydration of Leu/Arg97 residue in both copies. This material is available free of charge via the Internet at http://pubs.acs.org.

■ AUTHOR INFORMATION

Corresponding Author

*Tel: +4565503510. Fax: +4565504048. E-mail: hkhandel@memphys.sdu.dk.

Funding

H.K. is funded by a Lundbeck Junior Group Leader Investigator Fellowship.

Notes

The authors declare no competing financial interest.

■ ACKNOWLEDGMENTS

The computations were performed at the SDU node of the Danish Center for Scientific Computing (DCSC), the Joint Nordic Supercomputer in Iceland, Gardar, and HECToR: UK National Supercomputing Service. We thank Poul Nissen for fruitful discussions.

■ ABBREVIATIONS USED

NKA, Na^+,K^+-ATPase; APA, aldosterone-producing adenoma; MD, molecular dynamics; PDB, Protein Data Bank; RDF,

radial distribution function; PME, particle mesh Ewald; POPC, 1-palmitoyl-2-oleoyl-*sn*-glycero-3-phosphocholine

REFERENCES

(1) Skou, J. C. (1957) The influence of some cations on an adenosine triphosphatase from peripheral nerves. *Biochim. Biophys. Acta 23*, 439−446.

(2) Glynn, I. M. (2002) A hundred years of sodium pumping. *Annu. Rev. Physiol. 64*, 1−18.

(3) Morth, J. P., Pedersen, B. P., Buch-Pedersen, M. J., Andersen, J. P., Vilsen, B., Palmgren, M. G., and Nissen, P. (2011) A structural overview of the plasma membrane Na^+,K^+-ATPase and H^+-ATPase ion pumps. *Nat. Rev. Mol. Cell Biol. 12*, 60−70.

(4) Post, R. L., and Jolly, P. C. (1957) The linkage of sodium, potassium, and ammonium active transport across the human erythrocyte membrane. *Biochim. Biophys. Acta 25*, 118−128.

(5) Clausen, M. J., and Poulsen, H. (2013) Sodium/potassium homeostasis in the cell. *Met. Ions Life Sci. 12*, 41−67.

(6) Post, R. L., Hegyvary, C., and Kume, S. (1972) Activation by adenosine triphosphate in the phosphorylation kinetics of sodium and potassium ion transport adenosine triphosphatase. *J. Biol. Chem. 247*, 6530−6540.

(7) Albers, R. W. (1967) Biochemical aspects of active transport. *Annu. Rev. Biochem. 36*, 727−756.

(8) Morth, J. P., Pedersen, B. P., Toustrup-Jensen, M. S., Sorensen, T. L., Petersen, J., Andersen, J. P., Vilsen, B., and Nissen, P. (2007) Crystal structure of the sodium-potassium pump. *Nature 450*, 1043−1049.

(9) Shinoda, T., Ogawa, H., Cornelius, F., and Toyoshima, C. (2009) Crystal structure of the sodium-potassium pump at 2.4 Å resolution. *Nature 459*, 446−450.

(10) Ogawa, H., Shinoda, T., Cornelius, F., and Toyoshima, C. (2009) Crystal structure of the sodium-potassium pump (Na^+,K^+-ATPase) with bound potassium and ouabain. *Proc. Natl. Acad. Sci. U.S.A. 106*, 13742−13747.

(11) Laursen, M., Yatime, L., Nissen, P., and Fedosova, N. U. (2013) Crystal structure of the high-affinity Na^+,K^+-ATPase-ouabain complex with Mg^{2+} bound in the cation binding site. *Proc. Natl. Acad. Sci. U.S.A. 110*, 10958−10963.

(12) Morth, J. P., Poulsen, H., Toustrup-Jensen, M. S., Schack, V. R., Egebjerg, J., Andersen, J. P., Vilsen, B., and Nissen, P. (2009) The structure of the Na^+,K^+-ATPase and mapping of isoform differences and disease-related mutations. *Philos. Trans. R. Soc., B 364*, 217−227.

(13) Azizan, E. A., Poulsen, H., Tuluc, P., Zhou, J., Clausen, M. V., Lieb, A., Maniero, C., Garg, S., Bochukova, E. G., Zhao, W., Shaikh, L. H., Brighton, C. A., Teo, A. E., Davenport, A. P., Dekkers, T., Tops, B., Kusters, B., Ceral, J., Yeo, G. S., Neogi, S. G., McFarlane, I., Rosenfeld, N., Marass, F., Hadfield, J., Margas, W., Chaggar, K., Solar, M., Deinum, J., Dolphin, A. C., Farooqi, I. S., Striessnig, J., Nissen, P., and Brown, M. J. (2013) Somatic mutations in ATP1A1 and CACNA1D underlie a common subtype of adrenal hypertension. *Nat. Genet. 45*, 1055−1060.

(14) Beuschlein, F., Boulkroun, S., Osswald, A., Wieland, T., Nielsen, H. N., Lichtenauer, U. D., Penton, D., Schack, V. R., Amar, L., Fischer, E., Walther, A., Tauber, P., Schwarzmayr, T., Diener, S., Graf, E., Allolio, B., Samson-Couterie, B., Benecke, A., Quinkler, M., Fallo, F., Plouin, P. F., Mantero, F., Meitinger, T., Mulatero, P., Jeunemaitre, X., Warth, R., Vilsen, B., Zennaro, M. C., Strom, T. M., and Reincke, M. (2013) Somatic mutations in ATP1A1 and ATP2B3 lead to aldosterone-producing adenomas and secondary hypertension. *Nat. Genet. 45*, 440−444.

(15) Li, C., Capendeguy, O., Geering, K., and Horisberger, J. D. (2005) A third Na^+-binding site in the sodium pump. *Proc. Natl. Acad. Sci. U.S.A. 102*, 12706−12711.

(16) Poulsen, H., Khandelia, H., Morth, J. P., Bublitz, M., Mouritsen, O. G., Egebjerg, J., and Nissen, P. (2010) Neurological disease mutations compromise a C-terminal ion pathway in the Na^+/K^+-ATPase. *Nature 467*, 99−102.

(17) Poulsen, H., Nissen, P., Mouritsen, O. G., and Khandelia, H. (2012) Protein kinase A (PKA) phosphorylation of Na^+/K^+-ATPase opens intracellular C-terminal water pathway leading to third Na^+-binding site in molecular dynamics simulations. *J. Biol. Chem. 287*, 15959−15965.

(18) Einholm, A. P., Andersen, J. P., and Vilsen, B. (2007) Importance of Leu99 in transmembrane segment M1 of the Na^+,K^+-ATPase in the binding and occlusion of K^+. *J. Biol. Chem. 282*, 23854−23866.

(19) Musgaard, M., Thogersen, L., and Schiott, B. (2011) Protonation states of important acidic residues in the central Ca^{2+} ion binding sites of the Ca^{2+}-ATPase: A molecular modeling study. *Biochemistry 50*, 11109−11120.

(20) Law, R. J., Munson, K., Sachs, G., and Lightstone, F. C. (2008) An ion gating mechanism of gastric H,K-ATPase based on molecular dynamics simulations. *Biophys. J. 95*, 2739−2749.

(21) Wang, H. L., Cheng, X., Taylor, P., McCammon, J. A., and Sine, S. M. (2008) Control of cation permeation through the nicotinic receptor channel. *PLoS Comput. Biol. 4*, e41-1−e41-9.

(22) Sonntag, Y., Musgaard, M., Olesen, C., Schiott, B., Moller, J. V., Nissen, P., and Thogersen, L. (2011) Mutual adaptation of a membrane protein and its lipid bilayer during conformational changes. *Nat. Commun. 2*, 304.

(23) Berendsen, H. J. C., van der Spoel, D., and van Drunen, R. (1995) GROMACS: A message-passing parallel molecular dynamics implementation. *Comput. Phys. Commun. 91*, 43−56.

(24) Hess, B., Kutzner, C., Van Der Spoel, D., and Lindahl, E. (2008) GROMACS 4: Algorithms for highly efficient, load-balanced, and scalable molecular simulation. *J. Chem. Theory Comput. 4*, 435−447.

(25) Van Der Spoel, D., Lindahl, E., Hess, B., Groenhof, G., Mark, A. E., and Berendsen, H. J. C. (2005) GROMACS: Fast, flexible, and free. *J. Comput. Chem. 26*, 1701−1718.

(26) Pronk, S., Pall, S., Schulz, R., Larsson, P., Bjelkmar, P., Apostolov, R., Shirts, M. R., Smith, J. C., Kasson, P. M., van der Spoel, D., Hess, B., and Lindahl, E. (2013) GROMACS 4.5: A high-throughput and highly parallel open source molecular simulation toolkit. *Bioinformatics 29*, 845−854.

(27) Mackerell, A. D., Jr., Feig, M., and Brooks, C. L., 3rd (2004) Extending the treatment of backbone energetics in protein force fields: Limitations of gas-phase quantum mechanics in reproducing protein conformational distributions in molecular dynamics simulations. *J. Comput. Chem. 25*, 1400−1415.

(28) MacKerell, A. D., Bashford, D., Bellott, Dunbrack, R. L., Evanseck, J. D., Field, M. J., Fischer, S., Gao, J., Guo, H., Ha, S., Joseph-McCarthy, D., Kuchnir, L., Kuczera, K., Lau, F. T. K., Mattos, C., Michnick, S., Ngo, T., Nguyen, D. T., Prodhom, B., Reiher, W. E., Roux, B., Schlenkrich, M., Smith, J. C., Stote, R., Straub, J., Watanabe, M., Wiórkiewicz-Kuczera, J., Yin, D., and Karplus, M. (1998) All-atom empirical potential for molecular modeling and dynamics studies of proteins. *J. Phys. Chem. B 102*, 3586−3616.

(29) Bjelkmar, P. r., Larsson, P., Cuendet, M. A., Hess, B., and Lindahl, E. (2010) Implementation of the CHARMM force field in GROMACS: Analysis of protein stability effects from correction maps, virtual interaction sites, and water models. *J. Chem. Theory Comput. 6*, 459−466.

(30) Klauda, J. B., Venable, R. M., Freites, J. A., O'Connor, J. W., Tobias, D. J., Mondragon-Ramirez, C., Vorobyov, I., MacKerell, A. D., and Pastor, R. W. (2010) Update of the CHARMM all-atom additive force field for lipids: Validation on six lipid types. *J. Phys. Chem. B 114*, 7830−7843.

(31) Piggot, T. J., Piñeiro, Á., and Khalid, S. (2012) Molecular dynamics simulations of phosphatidylcholine membranes: A comparative force field study. *J. Chem. Theory Comput. 8*, 4593−4609.

(32) Jorgensen, W. L., Chandrasekhar, J., Madura, J. D., Impey, R. W., and Klein, M. L. (1983) Comparison of simple potential functions for simulating liquid water. *J. Chem. Phys. 79*, 926−935.

(33) Darden, T., York, D., and Pedersen, L. (1993) Particle mesh Ewald: An N·log(N) method for Ewald sums in large systems. *J. Chem. Phys. 98*, 10089−10092.

(34) Essmann, U., Perera, L., Berkowitz, M. L., Darden, T., Lee, H., and Pedersen, L. G. (1995) A smooth particle mesh Ewald method. *J. Chem. Phys. 103*, 8577−8593.
(35) Berendsen, H. J. C., Postma, J. P. M., Van Gunsteren, W. F., Dinola, A., and Haak, J. R. (1984) Molecular dynamics with coupling to an external bath. *J. Chem. Phys. 81*, 3684−3690.
(36) Nose, S. (1984) A unified formulation of the constant temperature molecular dynamics methods. *J. Chem. Phys. 81*, 511−519.
(37) Hoover, W. G. (1985) Canonical dynamics: Equilibrium phase-space distributions. *Phys. Rev. A 31*, 1695−1697.
(38) Parrinello, M., and Rahman, A. (1981) Polymorphic transitions in single crystals: A new molecular dynamics method. *J. Appl. Phys. 52*, 7182−7190.
(39) Nosé, S., and Klein, M. L. (1983) Constant pressure molecular dynamics for molecular systems. *Mol. Phys. 50*, 1055−1076.
(40) Damjanovic, A., Garcia-Moreno, E. B., and Brooks, B. R. (2009) Self-guided Langevin dynamics study of regulatory interactions in NtrC. *Proteins 76*, 1007−1019.
(41) Wolf, M. G., Hoefling, M., Aponte-Santamaria, C., Grubmuller, H., and Groenhof, G. (2010) g_membed: Efficient insertion of a membrane protein into an equilibrated lipid bilayer with minimal perturbation. *J. Comput. Chem. 31*, 2169−2174.
(42) Smart, O. S., Goodfellow, J. M., and Wallace, B. A. (1993) The pore dimensions of gramicidin A. *Biophys. J. 65*, 2455−2460.
(43) Humphrey, W., Dalke, A., and Schulten, K. (1996) VMD: Visual molecular dynamics. *J. Mol. Graphics 14*, 33−38.
(44) Berka, K., Hanak, O., Sehnal, D., Banas, P., Navratilova, V., Jaiswal, D., Ionescu, C. M., Svobodova Varekova, R., Koca, J., and Otyepka, M. (2012) MOLEonline 2.0: Interactive web-based analysis of biomacromolecular channels. *Nucleic Acids Res. 40*, W222−227.
(45) Shannon, R. (1976) Revised effective ionic radii and systematic studies of interatomic distances in halides and chalcogenides. *Acta Crystallogr., Sect. A 32*, 751−767.
(46) Ratheal, I. M., Virgin, G. K., Yu, H., Roux, B., Gatto, C., and Artigas, P. (2010) Selectivity of externally facing ion-binding sites in the Na/K pump to alkali metals and organic cations. *Proc. Natl. Acad. Sci. U.S.A. 107*, 18718−18723.
(47) Yu, H., Ratheal, I. M., Artigas, P., and Roux, B. (2011) Protonation of key acidic residues is critical for the K^+-selectivity of the Na/K pump. *Nat. Struct. Mol. Biol. 18*, 1159−1163.
(48) Bublitz, M., Musgaard, M., Poulsen, H., Thogersen, L., Olesen, C., Schiott, B., Morth, J. P., Moller, J. V., and Nissen, P. (2013) Ion pathways in the sarcoplasmic reticulum Ca^{2+}-ATPase. *J. Biol. Chem. 288*, 10759−10765.
(49) Einholm, A. P., Andersen, J. P., and Vilsen, B. (2007) Roles of transmembrane segment M1 of Na^+,K^+-ATPase and Ca^{2+}-ATPase, the gatekeeper and the pivot. *J. Bioenerg. Biomembr. 39*, 357−366.
(50) Einholm, A. P., Toustrup-Jensen, M., Andersen, J. P., and Vilsen, B. (2005) Mutation of Gly-94 in transmembrane segment M1 of Na^+,K^+-ATPase interferes with Na^+ and K^+ binding in E2P conformation. *Proc. Natl. Acad. Sci. U.S.A. 102*, 11254−11259.
(51) Toyoshima, C., Iwasawa, S., Ogawa, H., Hirata, A., Tsueda, J., and Inesi, G. (2013) Crystal structures of the calcium pump and sarcolipin in the Mg^{2+}-bound E1 state. *Nature 495*, 260−264.
(52) Winther, A. M., Bublitz, M., Karlsen, J. L., Moller, J. V., Hansen, J. B., Nissen, P., and Buch-Pedersen, M. J. (2013) The sarcolipin-bound calcium pump stabilizes calcium sites exposed to the cytoplasm. *Nature 495*, 265−269.
(53) Laursen, M., Bublitz, M., Moncoq, K., Olesen, C., Moller, J. V., Young, H. S., Nissen, P., and Morth, J. P. (2009) Cyclopiazonic acid is complexed to a divalent metal ion when bound to the sarcoplasmic reticulum Ca^{2+}-ATPase. *J. Biol. Chem. 284*, 13513−13518.